Hydrogen Bonding Features in Cholinium-based Protic Ionic Liquids from Molecular Dynamics Simulations.

Marco Campetella[a+], Andrea Le Donne[a], Maddalena Daniele[b], Lorenzo Gontrani[a], Stefano Lupi[c], Enrico Bodo[a*]

[a] *Chemistry Department, University of Rome "La Sapienza", Rome Italy*

[b] *INFN-LNF, Via Enrico Fermi 40, Frascati, Italy*

[c] *CNR-IOM and Department of Physics, University of Rome "La Sapienza", Rome Italy*

ABSTRACT

We explore the structure of a series of Protic Ionic Liquids based on the choline cation and amino-acid anions. In the series the length and the branching of the amino-acid alkyl chain varies. Ab-initio molecular dynamics, X-ray diffraction measurements and infrared spectra have been used to provide a reliable picture of the short range structure and of the short-time dynamic process that characterize the fluids. We have put special emphasis on the peculiar and complicated network of hydrogen bonds that stem from the amphoteric nature of the anion moiety. The use of ab-initio molecular dynamics allows us to calculate the "exact" charge density of the system and hence to obtain fairly accurate infrared spectra that, in turn, have been used to assign the experimental ones.

1. Introduction

Protic Ionic Liquids (PILs) [1-4] are among the most interesting members belonging to the broad class of materials called Ionic Liquids (ILs). PILs are formally obtained by the conventional reaction of a base with an acid. The resulting salt can be liquid at room

[*]Corresponding author: Dipartimento di Chimica, Università di Roma "La Sapienza", Piazzale A. Moro 5, 00185, Roma, Italy. Email: enrico.bodo@uniroma1.it

[+]Present address: Laboratoire LECIME, CNRS UMR-7575, Chimie-ParisTech, 11 rue P. et M. Curie, F-75231 Paris, France.

temperature (or more generally below 100°C) when lattice formation is frustrated by the complexity and sterical mismatch of the molecular constituents. Actually, lattice formation can be prevented rather easily by choosing molecular component that in their ionized state have a certain degree of charge delocalization and a sufficient difference in their steric dimensions. Probably the simplest component of the PILs class is ethylammonium nitrate that also turns out to be the first synthesized IL [5].

If the difference between the pKa's of the reagents is large enough (>6) the ensuing liquid is completely ionized. [6] On the other hand, if the difference in pKa is small (<4) [7] the resulting product is a mixture of an ionic and polar phase. In the latter case, phase separation can occur that will eventually nullify the properties traditionally ascribed to ILs such as negligible evaporation and chemical stability. Obviously, we are interested only in compounds that are completely ionized.

Despite the chemical simplicity of the synthesis and of the composing molecular ions, PILs show a complex structural and dynamical behavior due to the occurrence of nano-segregation phenomena[8,9] and the presence of a peculiar network of hydrogen bonds [10,11] whose strength obviously depends on the ionic partners and their relative acidity.

Due to the chemical variability of the molecular constituents and to the possibility of combining different anions and cations, the number of possible PILs is practically infinite. This extreme versatility has given them the reputation of "designer materials": it is possible to chemically change the cation/anion structure to finely tune their physical chemistry properties. Especially attractive is the possibility of creating fully biocompatible PILs. The adoption of such materials would provide new applications in pharmacological and biomedical research [12-15]. For this purpose, a new class of PILs has been synthesized in which the typical inorganic anion such as $[PF6]^-$, $[BF4]^-$, Br^-, Cl^-, has been replaced by organic amino acid (AA) anions [16] and the cation is a choline [17]. This set of PILs, given that both constituents appear in metabolic processes, is nontoxic [18-20], and represents a promising class of materials for a range of bio-related applications[21-24].

The possible mobility of the PILs proton that is exchanged during their formation has opened the way to the use of these compounds as conductive materials in a variety of electrochemical applications. [25-28]

The aim of the present work is to elucidate the short-range structure of 4 compounds based on AA anions coupled with choline cations ([Ch]+) with special focus on the H-bond features (see Figure 1). To pursue this aim we shall analyze in detail the result from molecular dynamics (MD) computations that are validated by comparing the computed properties (structure factors and IR spectra) with experimental determination. The 4 AAs are valine ([Val]), norvaline ([Nva]), leucine ([Leu]) and norleucine ([Nle]). Given the rather complex chemical morphology of the compounds we are dealing with, these systems have been treated reliably via *ab initio* molecular dynamics (AIMD) in order to avoid the bias due to the use of an empirical force field.

2. Methods

2.1 Computational methods

We have performed several AIMD simulations of system composed by an equal number of amino acid anions and $[Ch]^+$cations. Two different box sizes were simulated for each of the four compounds: the first one is made by 12 ionic couples with box side lengths around 15-16 Å, the second one is a much smaller model made by 3 ionic couples with box side length of about 10 Å (for more details see supporting information, Table S1).

For all systems, a pre-equilibration was performed employing classical molecular dynamics within periodic boundary conditions, using the AMBER program package[29] and the GAFF force field [30,31] for 2 ns in the NPT ensemble; the simulation temperature was set at 350 K. The difference between the final MD and experimental densities was less than 5%. The starting configurations yielded by this procedure were used as starting points for he *ab initio* molecular dynamics simulations. The systems have been modeled as described in ref. [32] using the program CP2K [33], the Quickstep module [34] and the orbital transformation [35] for faster convergence. The electronic structure was calculated by means of the PBE [36] functional, with an explicit Van der Waals correction that includes the empirical dispersion correction (D3) by Grimme [37]. MOLOPT-DZVP-SR-GTH basis sets and GTH pseudopotentials [38,39] were used. The timestep was set to 0.5 fs and the simulation temperature was set at 350 K using the Nose-Hoover thermostat [40] in order to slightly accelerate the dynamics that is very slow at ambient conditions due to the high viscosity of these systems. [17]

Production time for the MD simulation was between 36 and 60 ps (for further details see Table S1). The systems made by 3 ionic couples were used to compute the maximally localized Wannier centers [41]. From these simulations, the IR spectrum has been obtained using the Fourier transform of the autocorrelation function of the dipole moment. The simulations with 3 ionic couples were also used for the computations of the free energy profile along the oxygen-oxygen distance (that represent the main H-bond feature between anions and cations). One of the 3 O-O distances has been restrained using a harmonic potential (with 0.1 a.u. force constant) centered at increasing values between 2.2 and 4.0 Å in 37 points. In each point the MD was propagated for 10 ps. The O-O distance at each point has been collected as a function of time and the relative histogram has been built. The free energy has been computed using the weighted histograms analysis (WHAM). [42]

2.2 Experimental

The synthesis of the [Ch][AA] ILs has been reported in the literature by our group [17] and we shall not report here the details. Most ionic liquids are hygroscopic and water is an inevitable contaminant in the samples. As reported in ref. [17], in order to minimize water contamination, the synthetized liquids have been dried in vacuum for 24 h and the water content after dehydration was assessed by Karl Fischer moisture titrator to be 0.2 wt%. Since both the X-ray and the IR spectra have not been collected in dry conditions the water content might have increased slightly. Anyway, an indicator of a conspicuous presence of water in the sample would have been a low intensity first peak in the X-ray diffraction spectra due to the loss of long-range ordering in the fluid. As we shall see, this is not the case for our samples.

The large angle X-ray scattering experiments were performed at room temperature using the non-commercial energy-scanning diffractometer in the Department of Chemistry at the University 'La Sapienza' of Rome (Italian Patent No. 01126484-23 June, 1993). For a detailed description of instrument, and technique see refs. [43-46] and, specifically to these systems, ref [32]. The total intensity of the scattered radiation is generally expressed as two contributions: the independent scattering and the 'static structure factor' *I(Q)* (*Q* being the

transferred momentum) that is the structurally sensitive component due to interference. *I(Q)* originates from the Fourier transform of the atom-atom pair correlation functions:

$$I(Q) = 4\pi\rho_0 \sum_{i,j}^{N} x_i x_j f_i f_j \left[\int_0^{\infty} r^2 \left(g_{ij}(r) - 1\right) \frac{\sin Qr}{Qr} dr \right] \quad (1)$$

where ρ_0 is the bulk number density of the system, x_i are the numerical concentrations of the species and f_i the Q-dependent X-ray scattering factors. Both the experimental and theoretical structure functions have been multiplied by

$$M(Q) = \frac{f_N^2(0)}{f_N^2(Q)} e^{-0.01Q^2} \quad (2)$$

which is a factor that improves the curve resolution at high Q. In the plots, we shall always report the product $I(Q)M(Q)Q$.

Infrared spectra (reported in Fig. 10, 11 and 12, see also SI), have been collected in transmission from nearly 50 to 4000 cm^{-1}. Samples have been put in a cell closed by two optical windows (polyethylene for the far-IR and Irtran 7 for the mid-IR, respectively). The transmitted infrared radiation produced by a Globar source and modulated through an IFS-66v Bruker Michelson interferometer equipped with a Mylar and KBr beam-splitter, has been measured by a Pyroelectric (far-IR) and MCT (mid-IR) detectors. The absorption coefficient has been finally calculated through the ratio between the IR intensity transmitted by the sample over that transmitted by the empty cell.

3. Discussion and results

Few and very general structural data about these systems have been reported by us in a previous work [32] where we have shown how our MD simulations were able to grasp the short-range structure of the fluid. In another study by some of us [47] an empirical force field has been used to provide structural information on the [Ch][Nle] system at the mesoscopic scale. Here we will present a much more detailed analysis of the AIMD trajectories with a focus on the H-bonding features that play a key role in these liquids. In addition, we will present, for the first time, a comparison of the computed vibrational properties of the fluids with experimental IR spectra. The discussion is organized as follows: we begin by presenting a comparison of the structural data of one of the liquids

with experimental data [47] in order to validate the results of the simulation protocol. We will continue by presenting a thorough analysis of the H-bonding features. Finally, we will discuss the vibrational properties of the liquids and compare our theoretical findings to experimental data.

3.1 Structural features

In Figure 2 we report the total structure factor and its Fourier transform (the total radial distribution function) for the [Ch][Nle] system. The horizontal axes of the two sets of data are related by $Q=2\pi/r$. The theoretical data displayed are those obtained by convoluting over the radial distribution functions (eq. (1)) as calculated from the MD simulation of 12 ionic couples. The agreement between experiment and theory is very good over a wide range of distances though the theoretical data below 0.4 $Å^{-1}$ are unreliable due to the finite box size of our simulations. This fact also limits the range over which theoretical data are available in the radial distribution function (right side of Figure 2, black line). The features of the structure factor above 4 $Å^{-1}$ do not correspond directly to interatomic distances. The most interesting features lie in the intermediate range where, between 2.5 and 4 $Å^{-1}$, we can assign the peaks to intramolecular first-neighbor correlations that come, mainly, from the covalent bond distances between electron-rich atoms (O, N and C). Below 2.5 $Å^{-1}$ we have the features due to inter-molecular correlation. For example, the peak at 2.3 $Å^{-1}$ correlates well with the intermolecular O-O distance of 2.6 Å that is due to the O-O hydrogen bonds (vide infra). The structure factors for the other 3 liquids are very similar in shape to the one presented thereby telling us that the overall sort-range structural shape of the fluid is almost the same along the series of the 4 AA anions. Therefore, we will resort to more sensitive probes of the local short-range structure in order to differentiate the liquids behavior.

A further test on the reliability of the simulations presented here is shown in Figure S1 of the supporting information where we compare the radial distribution functions of the center-of-mass of the molecular constituents to those obtained with a classical potential and presented in ref. [47]. The overall average distances between cations in our simulation turns out to be around 6.4 Å and that between anions and cations around 5.8 Å. Both distances are compatible with those obtained with the classical force field. The profile for

the anion-anion center-of-mass radial distribution, instead, shows some interesting differences: the first maximum in our simulation is more structured and more short-ranged (5.5 Å) with respect to the classical force field simulations. As we shall show below this contact between anions represents an important structural feature of these liquids that implies an unusual attractive interaction between the anions.

In Figure 3 we report a set of selected, intra-molecular radial distribution functions (g(r)) in order to elucidate the short-range structure of the 4 liquids. The panel on the left shows the anion-cation O-O g(r) that presents a clear peak at 2.5-2.6 Å due to H-bonding between the oxygen atoms. In order to provide a measure of the strength of the coordination between the oxygen atoms we computed the running volumetric integral of the g(r) up to the first g(r) minimum at 3 Å. The resulting first neighbor coordination number turns out to be 0.78 for [Val], 0.74 for [Nva] and 0.94 for [Leu] and [Nle]. This tells us that the H-bond feature is stronger in [Leu] and [Nle] AA anions. A glimpse of the structural shapes that are induced by the above H-bond can be had by looking at Figure 4. For each of the 4 possible AA anions we report the spatial distribution functions (density) of the oxygen and hydrogen atoms of the choline cation surrounding the anion. The H-bond feature can be simply and pictorially visualized as taking place along the spatial regions connecting the heteroatoms of the AA anion to the iso-surfaces containing the H (in white) and O atoms (in red) of the hydroxyl. Each AA anion in the liquid forms single or multiple H-bonds that have different directions with respect to the carboxylate spatial orientation: the most vivid example is that of [Leu] where each terminal of the carboxylate can act as a proton acceptor in two different preferential directions, thus, giving rise to 4 peaks in the spatial hydrogen/oxygen density in its surroundings. If we assume that an H-bond exists between an anion and a cation when their oxygen atoms are found to lie within 3 Å and when the O-H-O misalignment angle does not exceed 40 degrees, we can simply count the total number of H-bonds along each of the 4 trajectories. The average numbers of O-O H-bonds turn out to be 3.1 for [Val], 6.7 for [Leu] and [Nva] and 8.1 for [Nle].

A rather trivial geometrical analysis (reported in the supporting information, Figure S2) allows us to say that the formed H-bonds, in all the liquids, have a marked preference for collinearity with only few bent occurrences with angles mostly below 20°.

Returning to Figure 3, the middle panel shows the interaction between the negatively charged carboxylate and the positively charged quaternary nitrogen of choline. This is a long-range interaction and provides an interesting structural feature that is ubiquitous in this kind of ionic liquids [48]. Despite being not a directional interaction as in the previous H-bond case, it nevertheless represents the main source of cohesive energy in the fluid. Indeed, for each of the 4 ionic liquids, the coordination number (i.e. the volumetric running integral of the g(r) of Figure 3 up to its first minimum) is between 4 and 5. This means that each AA anion, in addition to binding one of the cations through H-bond, coordinates at least other 4-5 cations by means of electrostatic energy (this value roughly agrees with a total anion-cation coordination number of 6.2 reported in ref. [47]).

The right panel of Figure 3 reports the interaction between the amino group on the AA anion and the hydroxyl one on the cation. The series of AA anions, as explored by our simulations, does not show a uniform behavior with respect to this interaction. For [Val] and [Nva] we clearly see the formation hydrogen bonds at the amino group, while the process is much less efficient for [Nle] and absent for [Leu]. The H-bond at the amino group, when present, has an acceptor-donor distance of 2.7 Å that, when compared to the O-O one with 2.6 Å, identifies a weaker interaction. In addition, the coordination numbers relative to this H-bond are much lower that those of the O-O bond and around 0.2. Counting the N-H···O H-bonds, we conclude that roughly only one anion out of five coordinates a cation via such interaction. The presence of this feature can be easily spotted also by looking in Figure 4 where the N-H···O coordination pattern can be seen for [Val] and [Nva], but not for the other two.

In conclusion, the structure of these liquids is mainly driven by electrostatics, as expected. Two main electrostatic interactions are at play and their features are very similar along the AA series:

- A strong coordinating H-bond between the carboxylate and the hydroxyl terminals. Except for [Val], more than half of the ionic couples are coordinated through this H-bond. The strength and the number of H-bonds follow the following order [Nle]>[Nva]~[Leu]>[Val]. This finding qualitatively agrees with the analogous case found in ref. [49] where the number of H-bonds increased with the alkyl chain length.

- A long-range electrostatic interaction that coordinates each anion to 4 additional cations that is mediated by the Coulomb attraction between the negative charge delocalized over the carboxylate oxygen atoms and the quaternary nitrogen of choline. No relevant differences are seen for this interaction along the AA series.

A third, less important, interaction exists in the [Val] and [Nva] compounds and consists in H-bonding features between the amino group and the cation hydroxyl.

All the above discussion has been focused on the assumption that the first neighbor contacts (as it normally is in ionic liquids) are those between cations and anions. One interesting question arises however when we look at the anion-anion distance distributions since, in these kind of PILs, anions can establish H-bonds between them through the interaction of the carboxylate with the amino group. Naively one could argue that since anions are charged species they repel each other, and that therefore the overall structure in the fluid should be characterized by a dynamic pattern of alternating charges. In other words, one might expect each anion to be surrounded by cations and vice versa. It is necessary, however, to consider two additional important effects that may alter this simplified view: (i) the high dielectric constant of the fluid that can effectively screen the charge centers at long range and (ii) the charge delocalization that weakens the electrostatic repulsion at short range.

The existence of like-charge molecular interactions in ionic liquids has already been noticed in imidazolium-based ILs [50] and in cholinium based ones [51] where the presence of H-bond driven, cationic complexes has been detected. [52] In these examples, it turns out that the cooperative effect of cation-cation H-O···H hydrogen bonds overcomes the Coulomb repulsion.

At difference with the above-mentioned studies, the cationic cholinium moiety is here, for the greatest part, tightly coupled to the hydroxyl of the anion and therefore unable to form H-bonds within itself. On the other hand, the presence of possible donor/acceptor sites on the anions, makes them able to form H-bonds with each other. Therefore, what we have in the present systems is a situation where part of the anions turn out to be connected by H-bonds, despite the electrostatic repulsion. As far as we know, this is the first time that theoretical evidence for the formation of anionic dimers in ILs through like-charge ion interactions is presented.

To highlight the anion-anion interaction, we report in Figure 5 the *g(r)* between the polar atoms of the anions. The O-O *g(r)* (red lines) clearly indicates a repulsive interaction between the negatively charged carboxylates. The N-N and N-O *g(r)* shapes, instead, indicate an attractive interaction with structured first neighbor contacts and, especially in the case of N-O, the peak that falls at 3 Å can indicate a weak H-bond. An example of this kind of anion-anion contact is further reported in Figure 6 where we show a snapshot of the [Ch][Nva] trajectory where two anions are clearly bound by two H-bonds.

3.2 Dynamic of the H-bonding features

As we have seen in the previous section, there are various kinds of H-bonds that are established in the fluid: the first and stronger ones are those between the hydroxyl (cation) and the carboxylate (anion). A smaller number of weaker H-bonds between the amino group (anion) and the hydroxyl has also been detected in our simulations, mostly for the [Ch][Val] and [Ch][Nva] liquids. A third possibility is the formation of weaker H-bonds between the amino group on the anion and the carboxylate of another anion.

To study the dynamics of these bonds we return to the [Ch][Nle] case where we can analyze the evolution of the acceptor-donor distances for the $O^{-}\cdots H—O$ (cation-anion) and $O^{-}\cdots H—N$ (anion-anion). In Figure 7 we report the evolution of 6 examples of H-bonds established between the carboxylate groups of the AA anions and the hydroxyl group. For each carboxylate, we report two distances that correspond to its two oxygen atoms. If we go through the 6 panels of Figure 7 in reading order we see the following situations:

1. (upper left panel) an anion coordinating two cations. The two distances at 2.6 Å (black and blue lines) clearly identify two H-bonds of the same carboxylate with two different hydroxyl groups. The other two distances (red and magenta lines) pertain to the second oxygen of the carboxylate. At about 50 ps one of the hydroxyl switches between the oxygen atoms of the carboxylate. For a scheme of such H-bond dynamics see Figure 8.
2. (upper middle and right panels) an anion coordinating one cation. In both cases within the first 10 ps, the hydroxyl exchanges between the two carboxylate oxygen atoms.

3. (lower left panel) another occurrence of a double H-bond where an anion coordinates two cations. The particular dynamic is different from situation 1) above and both hydroxyl switch between the carboxylate oxygen atoms during the simulation.
4. (lower middle panel) same situation as in 2).
5. (lower right panel) a single H-bond where we do not see a switching of the carboxylate atoms.

We conclude that, in the very limited time span of our simulations, we only see a partial dynamic of H-bond formation and dissociation. In particular, the ionic couples that are held together by H-bonds are stable during the simulations and the only dynamical changes that can be observed are merely switches between the carboxylate terminals. It is therefore important to remark that the present simulations do not allow us to determine the lifetime of the H-bonds binding an ionic couple and that we have not been able to collect statistically meaningful data on the dissociation/association rates of ionic couples that are presumably well into the hundreds ps regime.

Examples of the dynamics of the H-bonds formed between anions are reported in an analogous fashion in Figure 9. This time we can see an example of H-bond formation (in the upper left panel), an example of H-bond dissociation (in the upper right panel), one example of multiple H-bond coexistence (lower left panel) and, finally, an exchange of anions through the simultaneous formation/dissociation of a single H-bond (lower right panel).

A set of MD simulation has been carried out using smaller systems composed by only 3 ionic couples. Within these, much smaller, system the computation of free energy profiles by “umbrella sampling” is feasible. We have performed this analysis for [Leu], [Nle] and [Nva] where the number of H-bonds turned out to be greater. The free-energy profiles are reported in Figure S3 of the supporting information. The free energy content of the H-bond for each liquid turned out to be between 1.5 and 2.0 kcal/mol and the minimum distance around 2.6 Å.

3.3 Infra-red spectra and vibrational properties

In Figure 10 we report, as an example, the decomposed power spectrum of the [Ch][Val] liquid and we compare it to the experimental IR spectra (top panels). Although the power spectra value is indicative of the density of vibrational states, it does not provide a correct IR intensity that is obviously due to the dipole variation. Despite this, the position of the bands in the power spectra are indicative of which motions contribute to the IR spectra. A clear advantage of using power spectra as obtained from MD simulations over the typical (zero Kelvin) frequency evaluation with static *ab-initio* computations, is that anharmonic and temperature effects are naturally included. Therefore the data presented in Figure 10 have not been scaled. The computed power spectrum well matches the position of the main absorption bands in the experimental data. A general redshift of the computed power spectra can be noticed and it is due to the fact that the simulations have been carried out at 350 K as opposed to room temperature experiment. This redshift is very small and can be easily accounted for by scaling the power spectrum towards the blue using a uniform frequency scaling factor of 1.011. The first experimental band at 1600 cm^{-1} in the fingerprint region (left panels of Figure 10) corresponds to the stretching of the carboxyl C=O bonds and to the bending of the amino group (second and fourth row panels respectively). The second band at 1480 cm^{-1} is due to CH_n groups and in particular to CH_2 bending motions (third row panel). At high frequencies the match between the experiment and theory worsens. This is due to a series of systematic inaccuracies in our simulations: (i) the effect of the different temperature between experiments and simulation, (ii) the intrinsic inaccuracy of the PBE functional that has a well-known tendency to overestimate bond energies [53], and finally (iii) the inaccuracies in the motion of the light nuclei (H) whose "oscillations" are treated classically and that therefore can absorb much more vibrational energy that they do in the real system. These effect are especially visible on the C-H stretching experimental vibrational frequencies between 2800 and 3000 cm^{-1} that are blue-shifted in the theoretical data (third row) of a factor of 1.04. A faint trace of a structure around 3400 cm-1 can be spotted in the experimental profile. This feature is probably due to N-H stretching motions as shown by the theoretical power spectrum (fourth row). The broad structure that can be seen in the experimental spectrum, which encompass the C-H and N-H stretching regions, and that

extends from 2500 to 3600 cm^{-1}, is due to the cation hydroxyl stretching motion. The broad range of energies along which this motion can take place (that is induced by the presence of a strong H-bond) is well reproduced by the theoretical data although the centroid of the band is slightly red-shifted because of the higher temperature of the simulation and because of the PBE tendency to over-bind H-bonds (and therefore to red-shift the O-H stretching frequencies).

Similar discussions can be made for all the other 4 compounds (see supporting information, figures S4, S5 and S6), but for brevity, here we only show the high frequency region in Figure 11. In this plot, we have scaled the theoretical data with different scaling factors (reported in brackets) in order to perfectly match the experimental data. As we can see, apart for the rather small scaling, the simulations are perfectly able to describe the fluid behavior and the ensuing, complex H-bond network at play.

As we mentioned in the computational section, we have performed a series of MD simulation using a smaller number of ionic couples. Within this approach, the computation of maximally localized Wannier functions is feasible along a sufficient time span to compute the autocorrelation function of the electric dipole. The Fourier transform of this autocorrelation function yields the computed IR spectrum. We report an example of these computations in Figure 12 where we show the experimental and theoretical IR spectrum for the [Ch][Val] compound. The fingerprint region is almost perfectly reproduced by our calculations, while the high-energy region suffers from the same problems that we have already described for the power spectrum discussion. In particular, the broad O-H stretching band (that the experiments center at 3200 cm^{-1}) is red-shifted to 3000 cm^{-1} because of PBE over-binding. The same holds for the C-H absorption bands that appear between 2800-3000 cm^{-1} in experiment and turn out blue-shifted at 3000-3200 cm^{-1} in the calculation. The spectra for the other three compounds are very similar and are reported in the supporting information only (Figure S7, S8 and S9).

3.4 Conclusions

In this work we have explored, by means of computational and experimental methods, the short-range structure and the short-time dynamics of a homologous series of ionic

liquids made by coupling a choline cation to an AA anion. The series of AA anions is created by varying the AA side chain through [Val], [Nva], [Leu] and [Nle], so that the anions differ for the length and branching of the alkyl chain. The liquids have been synthetized and infrared spectra have been collected. For one of the liquids ([Nle]) the X-ray structure factor has also been measured. Ab-initio molecular dynamic has been carried out for the 4 compounds using the PBE functional and the Born-Oppenheimer approximation. The short-range structure of the fluids is fairly similar along the series and is characterized by a rather complex network of hydrogen bonding features. A strong H-bond binds the cations hydroxyl to the negatively charged carboxylate group of the anions. The longer the side alkyl chain is, the stronger and more numerous these H-bonds are. In addition, we have detected the existence of two other H-bonding features: the first one binds cations and anions and involves the amino and hydroxyl groups, the second acts between anions and involves amino and carboxylate groups. La latter is particularly interesting because its presence alters significantly the typical picture of the short-range structure of ionic liquids where the first neighbor distance between equally charged molecular ions is generally larger that the one between oppositely charged ions. Such like-charge, H-bond mediated interactions had already been detected in other ILs where they induce the local assembly of cationic complexes. For the first time, we show here, by theoretical evidence that such complexes of like charged species may also be formed between anions. In the present compounds, it turns out that the average first neighbor distance between anions is shorter than the ones between cations and anions and much shorter than that between cations. It is interesting to note that this feature does not occur in classical MD simulations thereby showing that an accurate treatment of the electronic degrees of freedoms (polarization and many-body effects) is crucial to grasp the details of the fluid structure.

The MD simulations have also been employed to compute the total dipole of the system and hence the infrared spectra which have been compared to experimental measurements. The “fingerprint” region is well reproduced by our calculations and part of the absorption spectra has been assigned. The accuracy of our computation worsens in the high frequency region and a match between experiments and theory has been obtained only using scaling factors to account for well known, deficiency of the computational scheme.

Fortunately, these issues produce a systematic mismatch between experiments and theory and we have been able to completely assign the high frequency region of the infrared spectrum.

Supporting Information

Simulation data; radial distribution functions of the [Ch][Nle] IL as compared to classical MD simulations; combined radial-angular distribution functions for H-bonds in [Ch][Val] and [Ch][Nle]; free energy profiles of the O-H-O H-bonds; power and infrared spectra (simulated vs measured) for all the ILs.

Acknowledgements

The authors gratefully acknowledge Prof Ruggero Caminiti (Sapienza University of Rome, Chemistry Department) for providing us with the experimental X-Ray diffraction patterns. The financial support from "La Sapienza" (grant n. RM116154CA141A23) is also acknowledged. EB and AL gratefully acknowledge the computational support of CINECA through grant IscrC_AAAOX and PRACE (grant n.2013091962).

[1] Greaves, T. L.; Drummond, C. J. Protic ionic liquids: evolving structure−property relationships and expanding applications, *Chem. Rev*. **2015**, *115*, 11379−11448.

[2] Bodo, E.; Sferrazza, A.; Caminiti, R.; Mangialardo, S.; Postorino P. A prototypical ionic liquid explored by ab initio molecular dynamics and Raman spectroscopy. *J Chem. Phys.*, **2013,** *139*, 144309.

[3] Belieres J.-F.; Angell, C. A. Protic ionic liquids: preparation, characterization, and proton free energy level representation- *J. Phys. Chem.* B, **2007**, *111*, 4926-4937.

[4] Greaves, T. L.; Ha, K.; Muir, B. W.; Howard, S. C.; Weerawardena, A.; Kirby N.; Drummond, C. J. Protic ionic liquids (PILs) nanostructure and physico chemical properties: development of high-throughput methodology for PIL creation and property screens. *Phys.Chem.Chem.Phys.* **2015**, *17*, 2357.

[5] Walden P. Ueber die molekulargrösse und elektrische leitfähigkeit einiger geschmolzenen Salze. *Bull. Acad. Imper. Sci. St. Pétersbourg.* **1914,** *6*, 405–422.

[6] Doi, H.; Song, X.; Minofar, B.; Kanzaki, R.; Takamuku, T.; Umebayashi, Y. A new proton conductive liquid with no ions: pseudo-protic ionic liquids. *Chem. Eur. J*., **2013,** *19*, 11522–11526.

[7] Stoimenovski, J.; Izgorodina, E. I.; MacFarlane, D. R. Ionicity and proton transfer in protic ionic liquids *Phys. Chem. Chem. Phys.*, **2010,** *12*, 10341–10347.

[8] Bodo, E.; Mangialardo, S.; Capitani, F.; Gontrani, L.; Leonelli, F.; Postorino, P. Interaction of a long alkyl chain protic ionic liquid and water *J. Chem. Phys*. **2014,** *140*, 204503/1-204503/10.

[9] Campetella, M.; Gontrani, L.; Leonelli, F.; Bencivenni, L.; Caminiti, R. Two different models to predict ionic-liquid diffraction patterns: fixed-charge versus polarizable potentials *Chem. Phys. Chem*. **2015,** *16,* 197-203.

[10] Fumino, K.; Fossog, V.; Stange, P.; Paschek, D.; Hempelmann, R.; Ludwig, R. Controlling the subtle energy balance in protic ionic liquids: dispersion forces compete with hydrogen bonds *Angew. Chem. Int. Ed.* **2015,** *54*, 2792–2795.

[11] Campetella, M.; Montagna, M.; Gontrani, L.; Scarpellini E.; Bodo, E.; unexpected proton mobility in the bulk phase of cholinium-based ionic liquids. new insights from theoretical calculations, *Phys. Chem. Chem. Phys.* **2017,** *19*, 11869-11880.

[12] Stoimenovski, J.; Dean, P. M.; Izgorodina, E. I.; MacFarlane, D. R. Protic pharmaceutical ionic liquids and solids: aspects of protonics. *Faraday Discuss*. **2012,** *154*, 335−352.

[13] Yu, Y.; Lu, X.; Zhou, Q.; Dong, K.; Yao, H.; Zhang, S.; Biodegradable naphthenic acid ionic liquids: synthesis, characterization, and quantitative structure–biodegradation relationship, *Chem. Eur. J.* ***2008,*** *14*, 11174–11182.

[14] Hough, W. L.; Smiglak, M.; Rodríguez, H.; Swatloski, R. P.; Spear, S. K.; Daly, D. Y.; Pernak, J.; Grisel, J. E.; Carliss, R. D.; Soutullo, M. D. et al. The third evolution of ionic liquids: active pharmaceutical ingredients. *New J. Chem.* **2007,** *31*, 1429−1436.

[15] Fukaya, Y.; Iizuka, Y.; Sekikawa, K.; Ohno, H. Bio ionic liquids: room temperature ionic liquids composed wholly of biomaterials, *Green Chem.* **2007,** *9*, 1155–1157.

[16] Fukumoto, K.; Yoshizawa, M.; Ohno, H.; Room temperature ionic liquids from 20 natural amino acids *J. Am. Chem. Soc*. **2005,** *127*, 2398−2399.

[17] Masci, G.; De Santis, S.; Casciotta, F.; Caminiti, R.; Scarpellini, E.; Campetella, M.; and Gontrani, L. Cholinium amino acid based ionic liquids: a new method of synthesis and physico-chemical characterization. *Phys. Chem. Chem. Phys* **2015,** *17*, 20687−20698.

[18] Hou, X.D.; Liu, Q.P.; Smith, T. J.; Li, N.; Zong, M.H. Evaluation of toxicity and biodegradability of cholinium amino acids ionic liquids *PLoS ONE* **2013,** *8*, 591451–7.

[19] Weaver, K. D.; Kim, H. J.; Sun, J.; MacFarlane, D. R.; Elliott, G. D. Cyto-toxicity and biocompatibility of a family of choline phosphate ionic liquids designed for pharmaceutical applications. *Green Chem*. **2012**, *12*, 507–513.

[20] Nockemann, P.; Thijs, B.; Driesen, K.; Janssen, C. R.; Van Hecke, K.; Van Meervelt, L.; Kossmann, S.; Kirchner, B.; Binnemans, K.; Choline saccharinate and choline acesulfamate: ionic liquids with low toxicities, *J. Phys. Chem. B* **2007,** *111*, 5254–5263.

[21] Plaquevent, J.-C.; Levillain, J.; Guillen, F.; Malhiac, C.; Gaumont, A.C. Ionic liquids: new targets and media for amino acid and peptide chemistry. *Chemical Reviews* **2008**, *108*, 5035–5060.

[22] Petkovic, M.; Ferguson, J. L.; Gunaratne, H. Q. N.; Ferreira, R.; Leitao, M. C.; Seddon, K. R.; Rebelo, L. P. N.; Pereira, C. S. Novel biocompatible cholinium-based ionic liquids-toxicity and biodegradability *Green Chem*. **2012,** *12*, 643–649.

[23] Tao, G. H.; He, L.; Liu, W. S.; Xu, L.; Xiong, W.; Wang, T.; Kou, Y. Preparation, characterization and application of amino acid-based green ionic liquids. *Green Chem*. **2006,** *8*, 639–646.

[24] Karton, A.; Brunner, M.; Howard, M. J.; Warr, G. G.; Atkin R. The high performance of choline arginate for biomass pretreatment is due to remarkably strong hydrogen bonding by the anion, *ACS Sustainable Chem. Eng.,* **2018,** DOI: 10.1021/acssuschemeng.7b04489.

[25] Matsuoka, H.; Nakamoto, H.; Susan, M. A. B. H.; Watanabe, M. Brønsted acid base and poly base complexes as electrolytes for fuel cells under non-humidifying conditions. *Electrochim. Acta* **2005**, *50*, 4015-4021.

[26] Nakamoto, H.; Watanabe, M. Brønsted Acid-Base ionic liquids for fuel cell electrolytes *Chem. Commun.* **2007**, *24*, 2539-2541.

[27] Timperman, L.; Skowron, P.; Boisset, A.; Galiano, H.; Lemordant, D.; Frackowiak, E.; Beguin, F.; Anouti, M. Triethylammonium bis(tetrafluoromethylsulfonyl)amide protic ionic liquid as an electrolyte for electrical double-layer capacitors *Phys. Chem. Chem. Phys*. **2012**, *14*, 8199-8207.

[28] Menne, S.; Pires, J.; Anouti, M.; Balducci, A. Protic ionic liquids as electrolytes for lithium-ion batteries. Electrochem. Commun. **2013**, *31*, 39-41.

[29] Case, D. A.; Darden, T. A.; Cheatham, T. E.; Simmerling, C.L.; Wang, J.; Duke, R. E.; Luo, R.; Walker, R. C.; Zhang, W.; Merz, K.M.; et al. *Amber 12,* 2012.

[30] Wang, J.; Wolf, R. M.; Caldwell, J. W.; Kollman, P.A.; Case, D. A.; Development and testing of a general amber force field. *J. Comp. Chem*. **2004,** *25*, 1157–1174.

[31]Wang, J.; Wang, W.; Kollman, P.A.; Case, D. A. Automatic atom type and bond type perception in molecular mechanical calculations. *J. Mol. Graph. Mod*. **2006,** *25*, 247-260.

[32] Campetella, M.; Bodo, E.; Montagna, M.; De Santis, S.; Gontrani, L. Theoretical study of ionic liquids based on the cholinium cation. Ab initio simulations of their condensed phases *J. Chem. Phys*., **2016,** *144*, 104504.

[33] Hutter, J.; Iannuzzi, M.; Schiffmann, F.; VandeVondele, J. CP2k: atomistic simulations of condensed matter systems, *WIREs Comput. Mol. Sci.* **2013,** *4*, 15–25.

[34] Vandevondele, J.; Krack, M.; Mohamed, F.; Parrinello, M.; Chassaing J.; Hutter, J. Fast and accurate density functional calculations using a mixed Gaussian and plane waves approach, *Comp. Phys. Comm.* **2005,** *167*, 103–128.

[35] VandeVondele, J.; Hutter, J. An efficient orbital transformation method for electronic structure calculations, *J. Chem. Phys.* **2003,** *118*, 4365–4369.

[36] Madsen, G.K.H. Functional form of the generalized gradient approximation for exchange: The PBE functional, *Phys. Rev. B,* **2007***, 75*, 1951081–5.

[37] Grimme, S. Semiempirical GGA-type density functional constructed with a long-range dispersion correction, *J. Comp. Chem.,* **2006,** *27*, 1787–1789.

[38] Goedecker, S.; Teter, M.; and Hutter, J.; Separable dual-space Gaussian pseudopotentials. *Phys. Rev. B* **1996,** *54*, 1703–1710.

[39] Hartwigsen, C.; Goedecker, S.; and Hutter, J.; Relativistic separable dual-space Gaussian pseudopotentials from H to Rn. *Phys. Rev. B* **1998,** *58*, 3641–3662.

[40] Hoover, W.G. Canonical dynamics: Equilibrium phase-space distributions. *Phys. Rev. A, **1985,** 31*, 1695–1697.

[41] Silvestrelli P. L.; Parrinello, M. *J. Chem. Phys*. **1999**, *111*, 3572–3580.

[42] Kumar, S.; Bouzida, D.; Swendsen, R. H.; Kollman, P. A.; Rosenberg, J. M. The weighted histogram analysis method for free-energy calculations on biomolecules. I. The method. *J. Comput. Chem.* **1992,** *13*, 1011–1021.

[43]Albertini, V. R.; Bencivenni, L.; Caminiti, R.; Cilloco, F.; and Sadun, C.; A new technique for the study of phase transitions by means of energy dispersive x-ray diffraction. Application to polymeric samples, *J. Macromol. Sc. B* **1996,** *35*, 199–213.

[44]Carbone, M.; Caminiti, R.; and Sadun, C.; Structural study by energy dispersive X-ray diffraction of amorphous mixed hydroxycarbonates containing Co, Cu, Zn, Al, *J. Mater. Chem.* **1996,** *6*, 1709–1716.

[45] Atzei, D.; Ferri, T.; Sadun, C.; Sangiorgio, P.; and Caminiti, R.; Structural characterization of complexes between iminodiacetate blocked on styrene-divinylbenzene matrix (Chelex 100 resin) and Fe(III), Cr(III), and Zn(II) in solid phase by energy-dispersive X-ray diffraction *J. Am. Chem. Soc.* **2001,** *123*, 2552–2558.

[46] Campetella, M.; Gontrani, L.; Bodo, E.; Ceccaci, F.; Marincola, C.; Caminiti, R. Conformational isomerisms and nano-aggregation in substituted alkylammonium nitrates ionic liquids: An x-ray and computational study of 2-methoxyethylammonium nitrate. *J. Chem. Phys.* **2013,** *138*, 184506.

[47] Russina O.; De Santis S.; Gontrani L.; Micro- and mesoscopic structural features of a bio-based choline-amino acid ionic liquid *RSC Adv*. **2016**, *6*, 34737-34743.

[48] Bodo E.; Gontrani L.; Caminiti R.; Benedetto A.; Ballone P. Amino acid anions in organic ionic compounds. An ab initio study of selected ion pairs; *J. Phys. Chem. B* **2014**, *118*, 2471-2486.

[49] Campetella, M., Macchiagodena, M., Gontrani, L., Kirchner, B. Effect of alkyl chain length in protic ionic liquids: an AIMD perspective. *Mol. Phys.* **2017**, *115*, 1582–1589.

[50] Knorr, A; Stange, P.; Fumino, K.; Weinhold, F.; Ludwig, F. Spectroscopic evidence for clusters of like-charged ions in ionic liquids stabilized by cooperative hydrogen bonding. *ChemPhysChem* **2016**, *17*, 458-462.

[51] Strate, A.; Niemann, T.; Ludwig, R. Controlling the kinetic and thermodynamic stability of cationic clusters by the addition of molecules or counterions *Phys. Chem. Chem. Phys*. **2017**, *19*, 18854

[52] Knorr, A.; Fumino, K, Bonsa; A.-M.; Ludwig, R. Spectroscopic evidence of 'jumping and pecking' of cholinium and H-bond enhanced cation–cation interaction in ionic liquids. *Phys. Chem. Chem. Phys*. **2015**, *17*, 30978-30982.

[53] Ernzerhof, M.; Scuseria, G. E.; Assessment of the Perdew–Burke–Ernzerhof exchange-correlation Functional. *J. Chem. Phys*. **1999,** *110*, 5029.

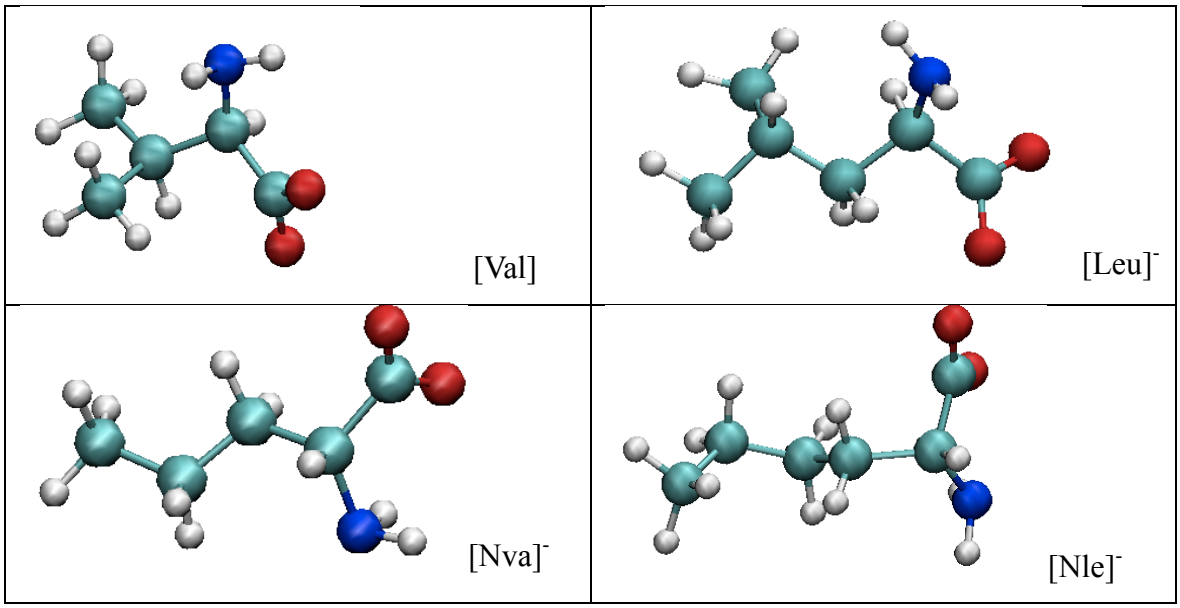

Figure 1: Molecular structures of the 4 amino anions.

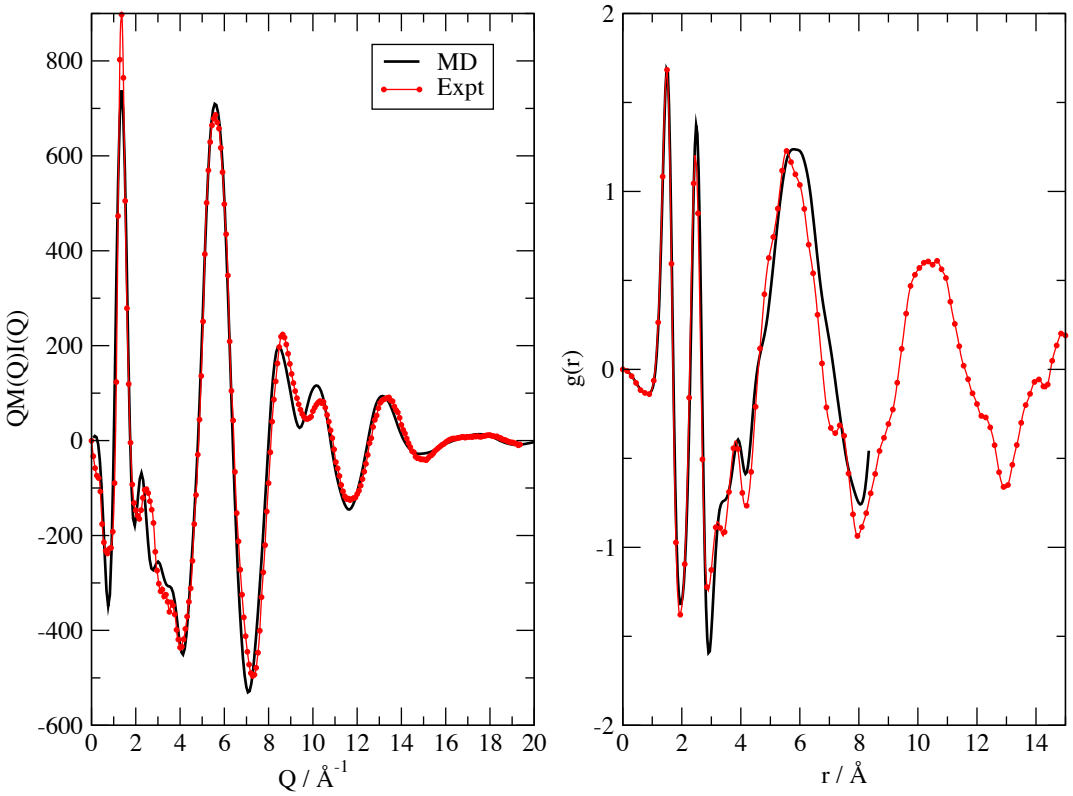

Figure 2: Left, I(Q)M(Q)Q as computed and measured for the [Ch][Nle] system. Right, Fourier transform of the data in the left. The latter represents the total radial distribution function of the system. The horizontal axes are related one to each other by r=2π/Q.

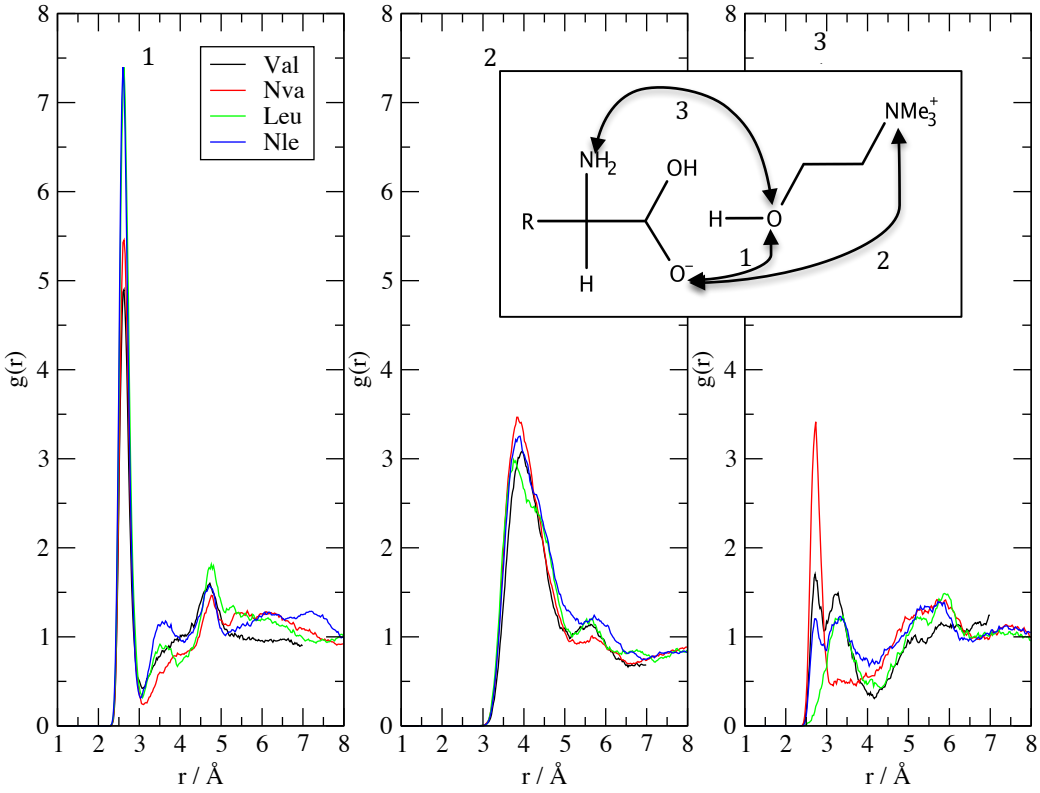

Figure 3: Selected intermolecular pair radial distribution functions *g(r)* for the 4 compounds. Left panel reports the O-O *g(r)* between anions and cations (interaction 1 in the inset). Middle panel reports the interaction between the carboxylate oxygens of anion and the quaternary nitro group of the cation (interaction 2 in the inset). The right panel reports the interaction between the AA anion nitro group and the hydroxyl group on the cation (interaction 3 in the inset).

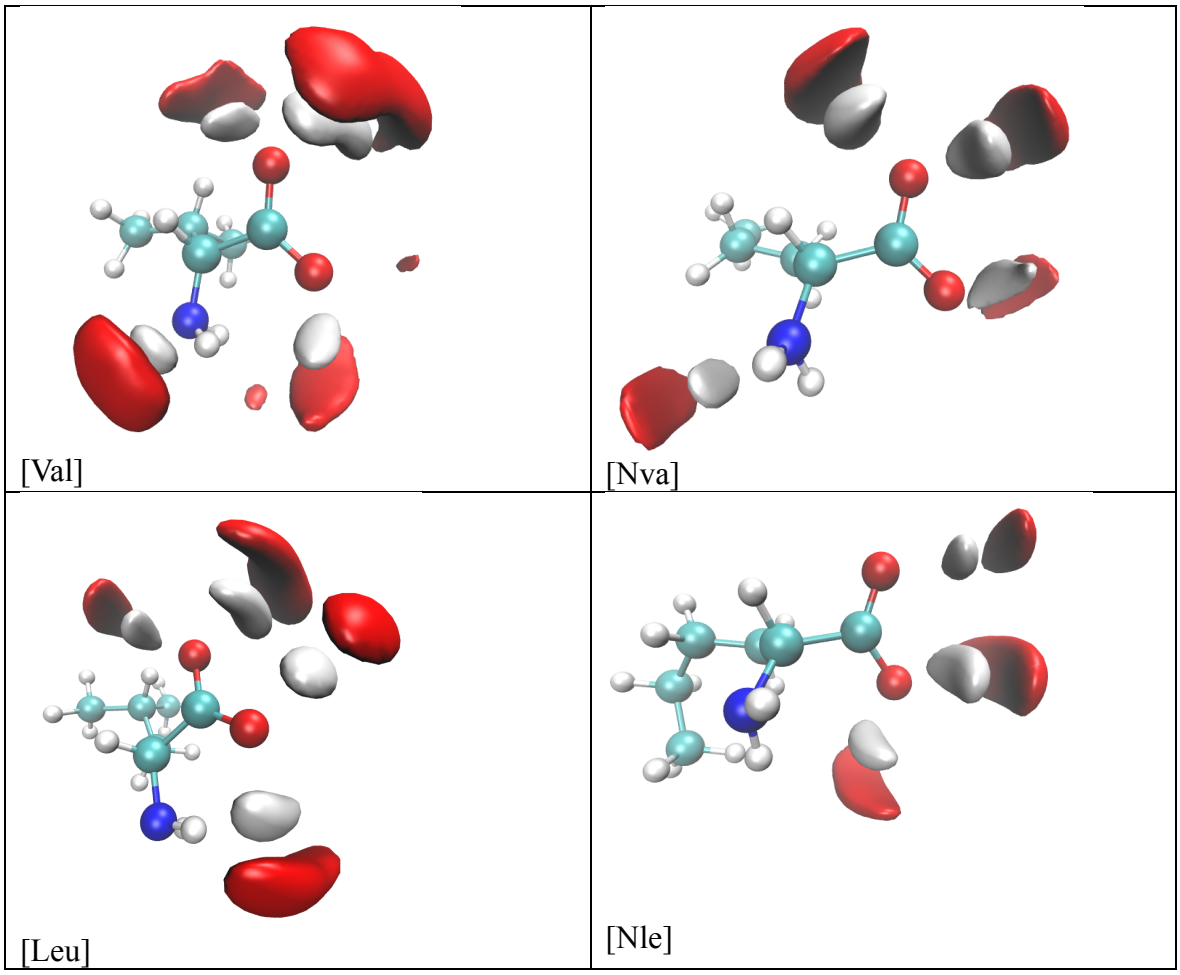

Figure 4: Spatial distribution functions relative to the possible hydrogen bonds. The SDF is built by fixing in space the CO_2^- group of each anion and plotting the oxygen (red) and hydrogen (white) density isosurface. The exact value of the isosurface depends on the compound, but it has been chosen as to include about 70% of the total element density. While the carboxylate is fixed in space, the geometry of the rest of the reference molecule is plotted only for illustration purposes.

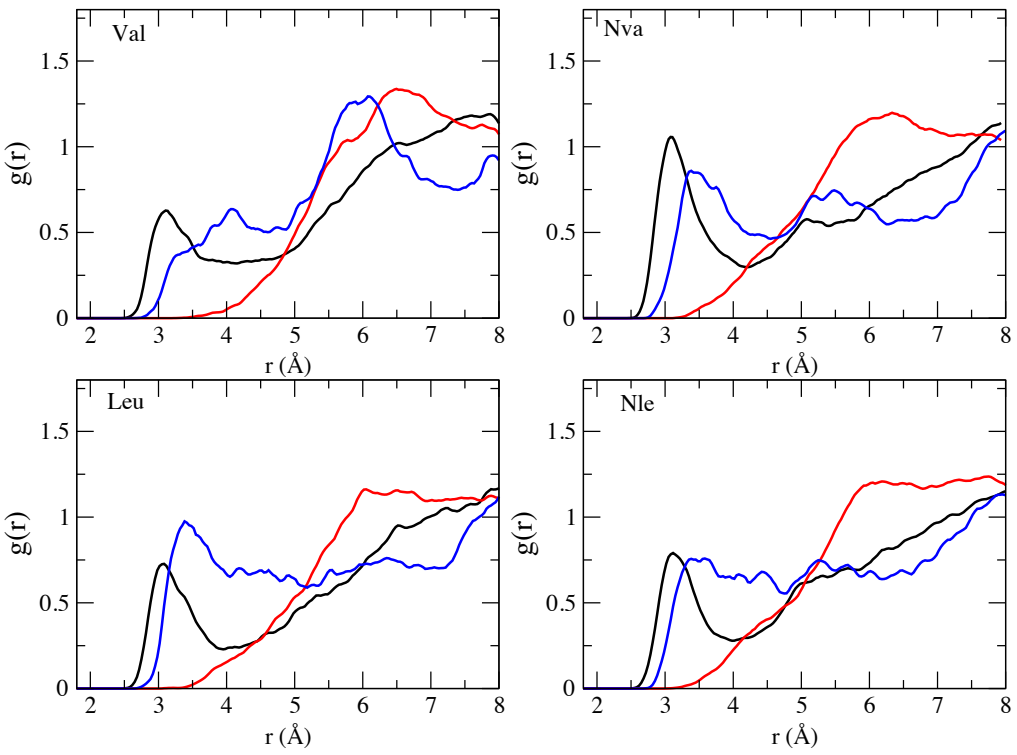

Figure 5: Anion-anion polar atom g(r). O-O in red, N-N in blue and N-O in black.

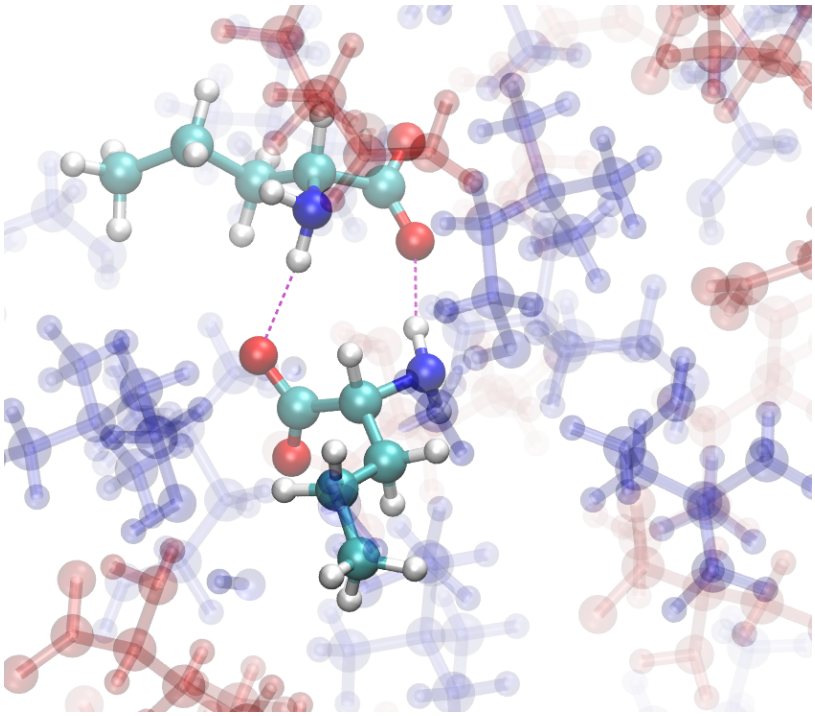

Figure 6: example of the occurrence of anion-anion H-bonds in the [Nva] PIL. Surrounding ions have been rendered transparent.

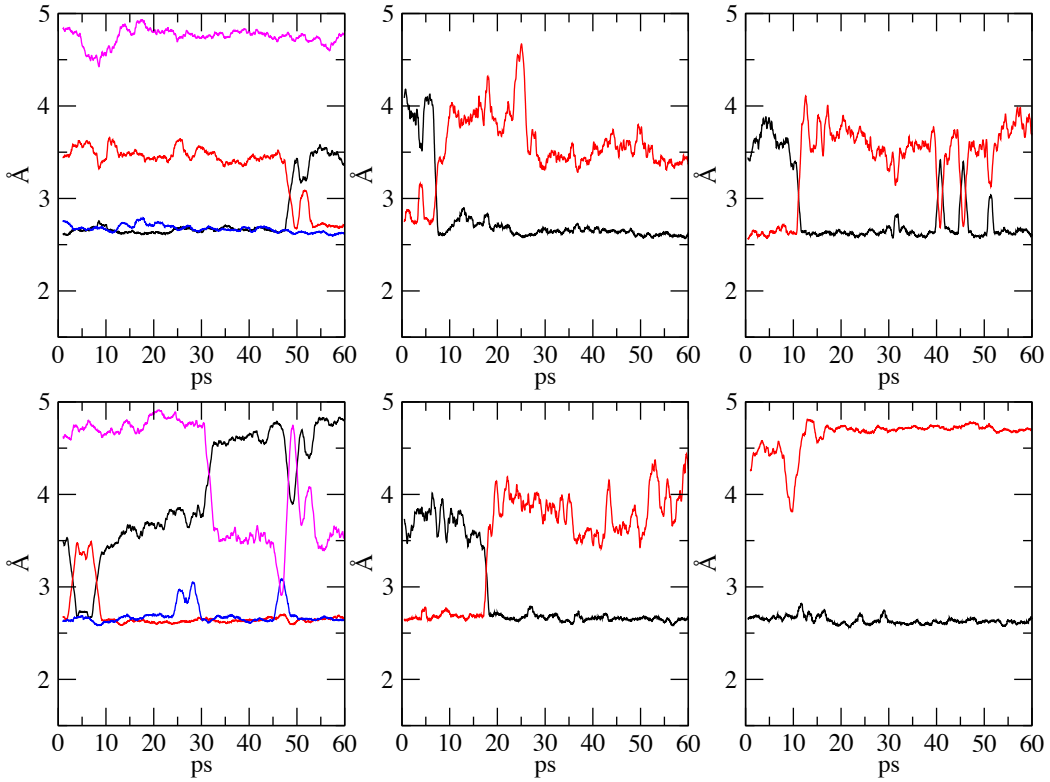

Figure 7: [Ch][Nle] liquid: temporal evolution of the acceptor-donor (Oxygen-Oxygen) distance in the CO_2^-···HO hydrogen bonds. The color code is the following: in black and red the two CO_2^- ···HO distances that pertain to the same hydroxyl. In blue and magenta the distances of the same carboxylate with the hydroxyl of a second cation.

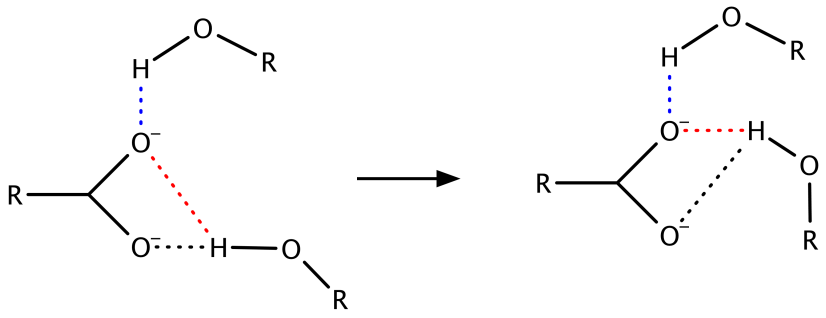

Figure 8: Scheme of the double H-bond dynamics.

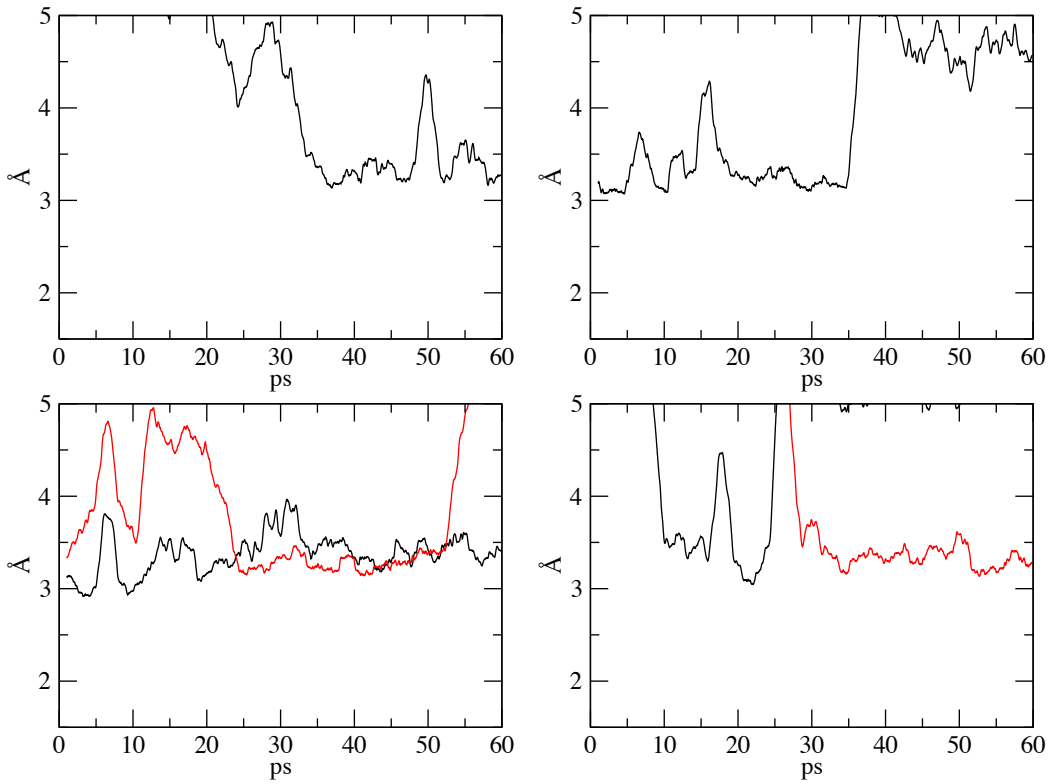

Figure 9: [Ch][Nle] liquid: temporal evolution of the acceptor-donor (Oxygen-Nitrogen) distance in the $CO_2^-\cdots H_2N$ hydrogen bonds. The two colors in the bottom panel refers to two different anions.

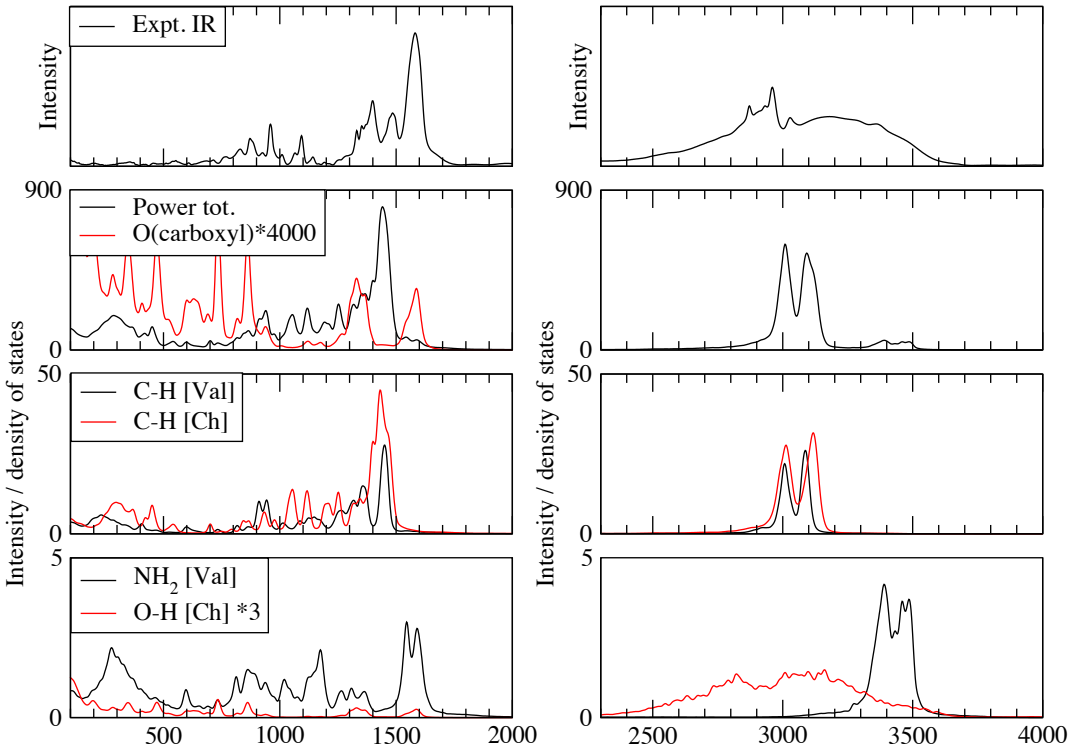

Figure 10: Power spectrum decomposition of [Ch][Val] compared with experimental IR spectra. Top panels: experimental data; second row: global power spectra and carboxyl oxygen; third row: C-H groups of anion and cation; bottom panels: amino group of anion and hydroxyl of cation.

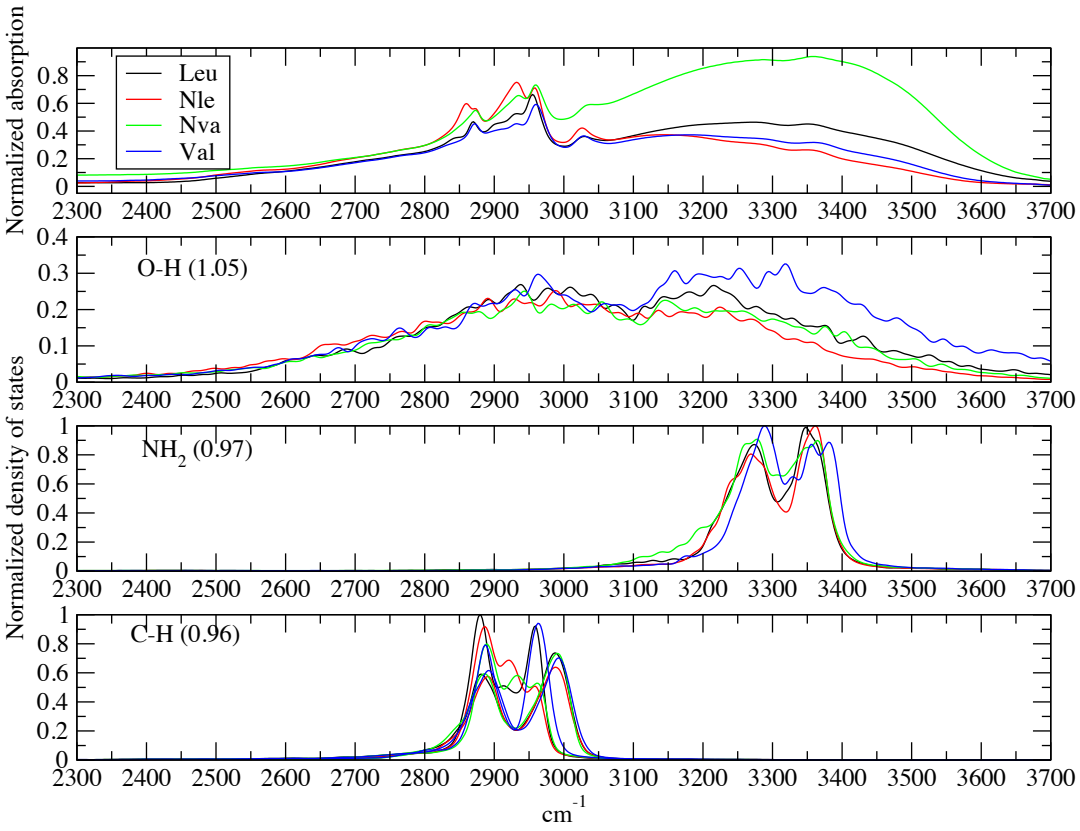

Figure 11: Decomposed power spectrum for the [Ch][Val], [Ch][Leu], [Ch][Nle] and [Ch][Nva] ionic liquids in the high frequency region. Experimental data in the top panel, theoretical calculations in the lower panels. For each group of atoms, a different scaling factor has been used as indicated in parenthesis.

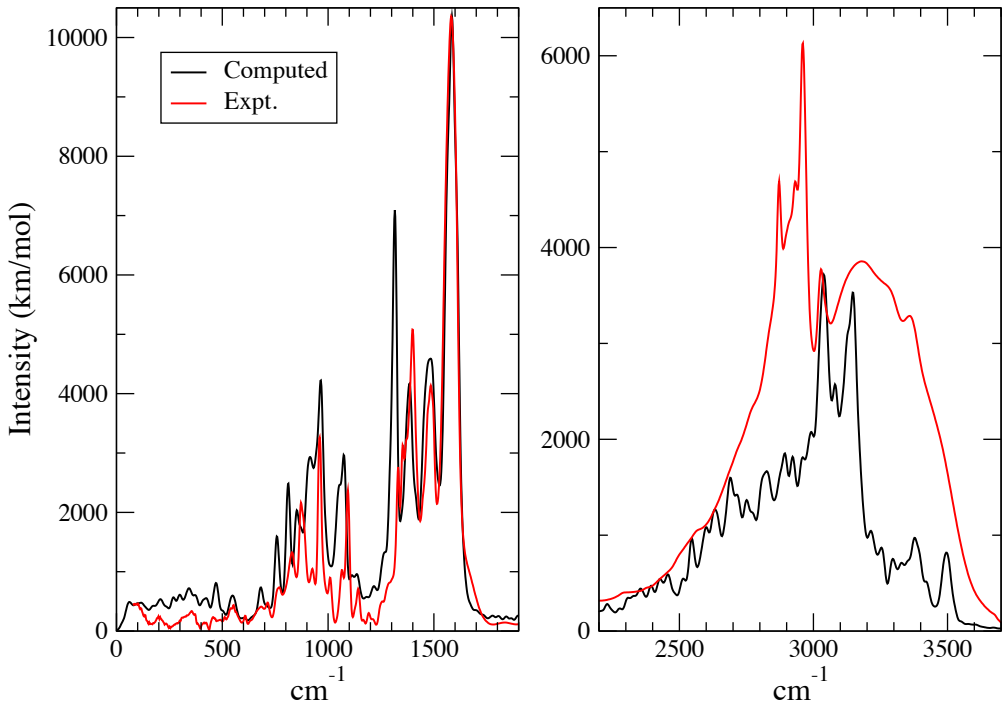

Figure 12: [Ch][Val] IR spectrum computed and calculated. The experimental data have been renormalized to match the computed absorption values. The theoretical data have been scaled by 1.011 to account for the different temperatures.

TOC graphic